

An overview of a highly versatile forward and stable inverse algorithm for airborne, ground-based and borehole electromagnetic and electric data

Esben Auken^{1,8} Anders Vest Christiansen¹ Casper Kirkegaard¹ Gianluca Fiandaca¹ Cyril Schamper² Ahmad Ali Behroozmand^{1,7} Andrew Binley³ Emil Nielsen⁴ Flemming Effersø⁵ Niels Bøie Christensen¹ Kurt Sørensen^{1,5} Nikolaj Foged¹ Giulio Vignoli^{1,6}

¹Department of Earth Sciences, Aarhus University, C.F. Møllers Allé 4, DK-8000 Aarhus C, Denmark.

²Sorbonne Universités, UPMC Univ Paris 06, 4 Place Jussieu, 75005 Paris, France.

³Lancaster University, Bailrigg, Lancaster LA1 4YW, UK.

⁴Danish Technical University, Anker Engelds Vej 1, Bygning 101A 2800 Kgs. Lyngby, Denmark.

⁵SkyTEM Surveys, Dyssen 2, DK-8200 Aarhus N, Denmark.

⁶Geological Survey of Denmark and Greenland (GEUS), Lyseng Allé 1, 8270 Højbjerg, Denmark.

⁷School of Earth Sciences, Stanford University, 397 Panama Mall, Mitchell Building, Suite 101, Stanford, CA 94305-2210, USA.

⁸Corresponding author. Email: esben.auken@geo.au.dk

Abstract. We present an overview of a mature, robust and general algorithm providing a single framework for the inversion of most electromagnetic and electrical data types and instrument geometries. The implementation mainly uses a 1D earth formulation for electromagnetics and magnetic resonance sounding (MRS) responses, while the geoelectric responses are both 1D and 2D and the sheet's response models a 3D conductive sheet in a conductive host with an overburden of varying thickness and resistivity. In all cases, the focus is placed on delivering full system forward modelling across all supported types of data. Our implementation is modular, meaning that the bulk of the algorithm is independent of data type, making it easy to add support for new types. Having implemented forward response routines and file I/O for a given data type provides access to a robust and general inversion engine. This engine includes support for mixed data types, arbitrary model parameter constraints, integration of prior information and calculation of both model parameter sensitivity analysis and depth of investigation. We present a review of our implementation and methodology and show four different examples illustrating the versatility of the algorithm. The first example is a laterally constrained joint inversion (LCI) of surface time domain induced polarisation (TDIP) data and borehole TDIP data. The second example shows a spatially constrained inversion (SCI) of airborne transient electromagnetic (AEM) data. The third example is an inversion and sensitivity analysis of MRS data, where the electrical structure is constrained with AEM data. The fourth example is an inversion of AEM data, where the model is described by a 3D sheet in a layered conductive host.

Key words: airborne electromagnetic, frequency domain electromagnetic, geoelectric, inversion, magnetic resonance sounding, transient electromagnetic.

Received 28 November 2013, accepted 26 May 2014, published online 29 July 2014

Introduction

A wide range of near-surface electric and electromagnetic geophysical measurement techniques are routinely employed for vastly different purposes within a variety of disciplines in modern science and engineering. Combining advanced forward modelling with sophisticated inversion schemes allows for obtaining accurate information on electric resistivity properties of geological layers, however, such algorithms are typically limited to the modelling of a single or a few types of data. Examples of this include:

- 1D inversion of frequency domain ground conductivity meter data (Santos, 2004),
- airborne frequency domain data in 1D (Sengpiel and Siemon, 2000),
- versatile inversion of frequency domain EM data in 1D (Oldenburg and Jones, 2011b),

- 1D holistic inversion of airborne frequency (Brodie and Sambridge, 2006a) and time domain EM data (Brodie and Sambridge, 2006b),
- 1D inversion of frequency and time domain data (Christensen and Auken, 1992),
- 1D approximate inversion of time domain data (Tartaras et al., 2000; Christensen, 2002; Macnae et al., 1991),
- 1D inversion of multiple types of time domain data (Oldenburg and Jones, 2011c),
- 3D inversion of airborne time and frequency domain data (Newman and Alumbaugh, 1997; Cox et al., 2010, Oldenburg et al., 2013),
- 2D inversion of resistivity (electrical resistivity tomography, ERT) and induced polarisation (IP) data (Loke and Barker, 1996; Loke et al., 2006; Oldenburg and Li, 1994, Fiandaca et al., 2013),
- 3D inversion of ERT data (Günther et al., 2006; Rücker et al., 2006),

- 3D inversion of ERT data with IP (Yoshioka and Zhdanov, 2005; Loke, 2011; Oldenburg and Jones, 2011a),
- 3D inversion of magnetotellurics data (Gribenko et al., 2010),
- inversion of magnetic resonance soundings (MRSs) recovering water content (Mohnke and Yaramanci, 2002; Mueller-Petke and Yaramanci, 2010; Hertrich et al., 2005)

Implementing just the base of such inversion algorithms can be a tremendous task in itself and often resources will limit the stage of development that can be reached. For this paper we present a more unusual research algorithm, AarhusInv, in the sense that it supports a broad spectrum of data types. AarhusInv has further been allowed to reach a point of production maturity, while at the same time being very actively developed for various research projects. Reaching this stage has to a large degree been made possible by support from the ongoing Danish national mapping of groundwater resources (Thomsen et al., 2004; Møller et al., 2009). This project was initiated in the late 1990s and has provided stable funding and extensive production use of the algorithm, including inversion of ERT data, PACES (Sørensen et al., 2005), ground-based TEM and airborne SkyTEM data (Sørensen and Auken, 2004). Furthermore, there have been many contributions on various parts of the algorithm, hence the long list of co-authors on this paper.

The main distinction to other algorithms reported in the literature is how different high accuracy forward models, spanning multiple data types, are brought together in a common inversion framework. This framework is not only optimised for production but also flexible for research, by supporting arbitrary spatial constraints and full integration of *a priori* information on any model parameter.

AarhusInv is freely available for university research institutions. Over time, it has been used for the inversion of an extensive amount of vastly different datasets, collected over all continents of the world. Some of the most prominent include an 18 000 line km Versatile Time-domain ElectroMagnetic (VTEM) survey conducted over the Okavango delta, Botswana (Podgorski et al., 2013); a 34 000 line km SkyTEM survey in the Broken Hill area of Australia in 2009; a 14 000 line km survey in India in 2013; and a 1000 line km TEMPEST survey on Eyre peninsula of South Australia (Auken et al., 2009a). For the Danish groundwater mapping project it has been used for inversion of ~40 000 ground-based TEM soundings, 25 000 line km of SkyTEM and several thousand ERT profiles. We estimate that the algorithm has inverted more than 400 000 line km of airborne data since 2005, including data from the Resolve system (Fugro Inc.), DigHEM (Fugro Inc.), SkyTEM (Sørensen and Auken, 2004), VTEM (Witherly et al., 2004), AeroTEM (Balch et al., 2003) and TEMPEST (Lane et al., 2000).

In this paper, we provide a review of the numerical implementation and demonstrate its flexibility and capabilities through examples. A core component is a constrained model framework which has proven successful for many different geologies, ranging from mapping of paleo channels in sedimentary environments to mapping of perched aquifers in a weathered volcanic geology (Jørgensen and Sandersen, 2006; d'Ozouville et al., 2008; Danielsen et al., 2003; Reid et al., 2007; Siemon et al., 2002). We begin by describing the design of the algorithm along with a list of supported data types and instrument geometries. This is followed by a review of the forward and inverse modelling schemes. Finally four field data examples illustrate the algorithms versatility to operate on data collected on the ground, in the ground and in the air.

Methodology

Modular algorithm layout

Since the origin of AarhusInv in 1995–1997, its feature set has evolved significantly, but in its simplest form the functionality is still to invert a set of geophysical soundings for a set of layered 1D models connected through constraints. The algorithm was formerly known as em1dinv, but with the introduction of multidimensional responses we changed the name to AarhusInv in 2012. The code base is in Fortran 95/77 and the program itself is a command line application with no user interface and with all input/output conducted through ASCII files. This structure is flexible and very well suited for functioning as an integrated inversion engine, as in the case of the front end GUI applications Aarhus Workbench (Auken et al., 2009c), EMMA (Auken et al., 2002) and SPIA (www.hgg.au.dk). The algorithm is implemented in a general modular manner as conceptually outlined in Figure 1. This figure is supplemented by Table 1, providing full details on supported data types, measurement geometries, and key references.

Starting from the top in Figure 1 a general model input file of flexible format is read first. This model file contains a starting model definition, specifies arbitrary regularisation constraints and holds prior information. Following model file input is the reading of data files in the data file input module. These files are encoded in data type specific formats, which are transparently

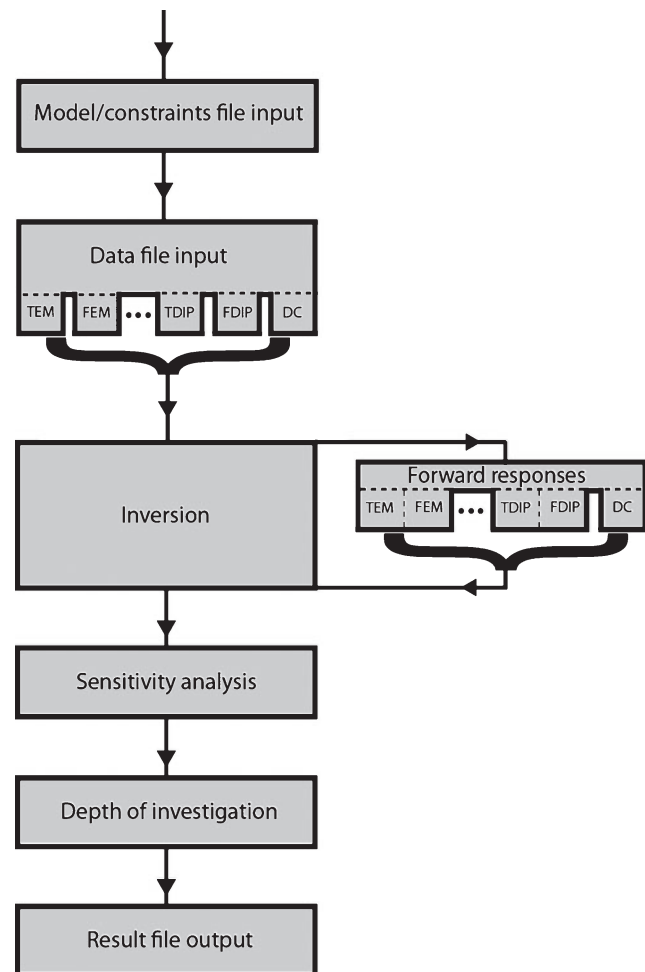


Fig. 1. Illustration of the modular algorithm design. All modules are implemented in a general manner to support any data type, except for the data file input and forward response modules which contains data type specific branches.

Table 1. Overview of supported data types and configurations. All time domain responses can be calculated as step or impulse response or with an arbitrary waveform.

1D, 2D and 3D are the dimensionalities of the response; E is electric field; H is magnetic field; $E_x, E_y, E_z, H_x, H_y, H_z$ are the x, y and z are the principal components of the electric and magnetic fields; DC is direct current (geoelectric), DC/IP is DC with time domain induced polarisation; MRS is magnetic resonance sounding. Key references for the basic electromagnetic calculations include ¹Ward and Hohmann (1988), ²Wannamaker et al. (1984), ³Xiong (1989). DC/IP responses in 1D are described by ⁴Zhdanov and Keller (1994) and ⁵Fiandaca et al. (2012) with the special case of electrodes in the layered half-space which follows ⁶Sato (2000). 2D DC/IP uses a generalisation of the approach described by ⁷Kemna et al. (2000) and is reported by ⁸Fiandaca et al. (2013). Sheets follow the theory of ⁹Weidelt (1983) and the implementation by ¹⁰Zhou (1989) with an additional time transform as discussed in ¹¹Schamper et al. (2013). MRS follows the equations in ¹²Weichman et al. (2000) and is reported in ¹³Behroozmand et al. (2012b). Surface wave seismics are reported in ¹⁴Wisén and Christiansen (2005).

Source group	Source type	Supported 1D responses			
		Receiver type	Source position	Receiver position	Domain
Dipole ^{1,2,3}	Vertical magnetic dipole	Dipole: Any E and H field component	Anywhere	Anywhere	Frequency and time
	Vertical electric dipole	Dipole: Any E and H field component	Anywhere	Anywhere	Frequency and time
	Horizontal electric dipole	Dipole: Any E and H field component	Ground surface or in the air	Anywhere	Frequency and time
	Horizontal magnetic dipole	Dipole: Any E and H field component	Ground surface or in the air	Ground surface or in the air	Frequency and time
Loop ^{1,2,3}	Rectangular loop	Dipole: Any E and H field component	Ground surface or in the air	Anywhere	Frequency and time
	Arbitrary segmented loop	Dipole: Any E and H field component	Ground surface or in the air	Anywhere	Frequency and time
	Circular centre	Dipole: H_z	Ground surface or in the air	Anywhere on the axis	Frequency and time
	Circular offset	Dipole: E_x, E_y, H_x, H_y, H_z	Ground surface or in the air	Anywhere	Frequency and time
Wire ^{1,2,3}	Circular in-loop	H_z	Ground surface or in the air	Ground surface or in the air	Frequency and time
	Finite length grounded x -directed dipole	Dipole: E_x, E_z, H_y, H_z (or B)	Ground surface	Anywhere	Frequency and time
	Finite length grounded y -directed dipole	Dipole: E_y, E_z, H_x, H_z (or B)	Ground surface	Anywhere	Frequency and time
	Infinite x -directed line source	Dipole: E_x, H_y, H_z (or B)	Ground surface	Anywhere	Frequency and time
DC ^{4,5,6}	Infinite x -directed line source	Dipole: E_y, H_x, H_z (or B)	Ground surface	Anywhere	Frequency and time
	Schlumberger	Apparent resistivity or potentials	Ground surface	Ground surface	
	Wenner	Apparent resistivity or potentials	Ground surface	Ground surface	
	Pole-pole	Apparent resistivity or potentials	Ground surface	Ground surface	
	Arbitrary quad pole	Apparent resistivity or potentials	Ground surface	Ground surface	
	Arbitrary quad pole in the ground	Apparent resistivity or potentials	Electrodes at the surface or in the ground	Electrodes at the surface or in the ground	
DC/IP ^{7,8}	Arbitrary quad pole in cylinder symmetry	Apparent resistivity or potentials	Electrodes in the ground	Electrodes in the ground	
	Arbitrary quad pole	Apparent resistivity/chargeability or potentials	Ground surface	Ground surface	Time domain
Magnetotelluric ¹	Arbitrary quad pole in the ground	Apparent resistivity/chargeability or potentials	Electrodes at the surface or in the ground	Electrodes at the surface or in the ground	Time domain
	MRS ^{12,13}	Apparent resistivity or dipole E_x, E_y, H_x, H_y		Ground surface or in the ground	
Surface wave dispersion ¹⁴	Arbitrary segmented loop		Ground surface	Ground surface	
Supported 2D and 3D responses					
Source group	Source type	Receiver type	Source position	Receiver position	Domain
DC/IP (2D) ^{7,8}	Arbitrary quad poles	Apparent resistivity/chargeability or potentials	Ground surface	Ground surface	Time
Loop – thin sheets (3D) ^{9,10,11}	Arbitrary segmented loop	Dipole: Any E and H field component	Ground surface or in the air	Anywhere	Frequency and time

handled by the modules internal branching to the relevant sub modules. Note that mixing of any number of different data types is supported, allowing for unrestricted joint inversions. Having filled the internal data structures from input files these structures are passed on to the general inversion module which starts the iterative inversion process. During the iterative course of minimising the residual the inversion module calls the forward response module (see Appendix A) for the calculation of forward response updates and derivatives. The forward response module also handles data type specific branching transparently, simply performing the requested calculations and returning the result to the inversion module. Internally, the forward response module makes data type dependent calls to a library of common routines. Having iteratively solved the inverse problem (see next paragraph and Appendix B) the result is sent to the general model analysis module, which calculates a model parameter sensitivity analysis. Finally the depth of investigation (DOI) is calculated based on the actual model output from the inversion process and a recalculated sensitivity (Jacobian) matrix (Christiansen and Auken, 2012). Following the DOI calculation a result file is finally written in a general file format.

Forward modelling

From a forward modelling point of view AarhusInv provides a wide range of options for simulating a given measurement system. This is particularly important for TEM data, as neglecting the influence of system parameters such as geometry, waveform or filters can lead to serious modelling error as described for TEM by Christiansen et al. (2011) and Fiandaca et al. (2012) for DC/IP. The extent to which the algorithm allows for full system forward modelling is relatively unique and makes it possible to compare model results from different data types as directly as possible. Key references for the forward modelling are given in the caption of Table 1. It is outside the scope of this paper to describe all these different solutions and therefore we have in Appendix A chosen to give descriptive details on the 1D EM solutions which are also the most used parts of AarhusInv.

The forward modelling is implemented parallel using OpenMP and scales close to linearly running on 1–64 processors. All vectors and matrices are furthermore implemented sparsely making the memory consumption relatively low even for very large inverse problems. It is out of the scope of this paper to describe the details of this implementation and we therefore refer to Kirkegaard and Auken (2014) for all details.

Inverse modelling

The mathematical formalism of the inverse modelling scheme follows the established practice by Menke (1989). Details are provided by Auken et al. (2005) and Appendix B gives in-depth details to the implementation of the inversion. Here, we focus on presenting the flexibility and capabilities of the algorithm. Essentially, we use a Gauss-Newton style

minimisation scheme with a Marquardt modification (Marquardt, 1963) to find the set of model parameters that minimise the L_2 misfit with respect to observed data, regularising and prior information. All datasets are inverted simultaneously, minimising a common object function. Consequently, the output models are balanced between the constraints, the physics and the data. Model parameters that have little influence on the data will be controlled by the constraints, and vice versa. The use of, for example, lateral or spatial constraints on a collection of models allows for information to propagate across a survey area.

Model constraints are applied between any two parameters of the same type by specifying the variance of the difference between the two and the uncertainty of prior information is similarly specified by the variance of the given prior value. The AarhusInv implementation itself is unbiased in terms of how constraints should be defined and thus leaves this to be specified by the user in the input model file. This format allows for arbitrary constraints linking any model parameters, i.e. a set of 1D models can be linked by 3D constraints in any way. Typically, we apply constraints in the form of 1D laterally constrained inversion (LCI; Auken et al., 2005) and 1D spatially constrained inversion (SCI; Viezzoli et al., 2008) for producing quasi 2D and quasi 3D models, respectively. The constraining formulation is flexible and allows for constraints and prior information on both primary and secondary model parameters. We define primary model parameters as the actual parameters of the layered model, e.g. resistivities and thicknesses, whereas secondary model parameters are any parameters that can be derived from linear combinations of the primary parameters, e.g. depths and elevations (Auken et al., 2005). This can be utilised for example when integrating prior information from a borehole, where the known parameter is typically the depth of a layer interface and not a layer thickness.

For the inversion of airborne data we allow including the instrument altitude as a model parameter, as will be discussed in more detail in the airborne example. In the case of helicopter data the pilot attempts to follow the terrain topography and maintains a relatively constant altitude, whereas in fixed wing surveys the aircraft typically operate at almost constant elevation. In this case it is desirable to supply lateral constraints linking the modelled instrument elevation of neighbouring models, instead of linking the primary model parameters in the form of height above terrain. Table 2 shows which additional model parameters are included in the inversion for certain airborne systems. These parameters are all in excess of the primary and secondary parameters of resistivity, thickness and depth.

In conjunction with any inversion result a model parameter analysis can be calculated, obtaining estimates of the resulting model uncertainty. This is done by calculating the covariance matrix of the resulting model of the inversion (Tarantola and Valette, 1982a, Auken and Christiansen, 2004), which provides a linearised error estimate. Since we perform our inversion in logarithmic model space for numerical stability, the values

Table 2. Additional inversion model parameters for relevant system types. The base model parameterisation includes resistivity, thickness and depth.

System type	Optional inversion parameters	
	Additional parameters	Purpose
All airborne TEM system	Receiver altitude/elevation	Correction for inaccurate determination of altitude
All airborne TEM systems	Data shift	Correction of data level
Fixed wing TEM systems	Receiver pitch roll and position	Correction for bird pitch, roll and position
MRS	Water content, T_2^* and stretch parameter (T_2^* distribution)	Additional parameters in model space
DC/IP	Chargeability, C and time constant (Cole-Cole parameters)	Additional parameters in model space
Sheets	Sheet position, size, strike and dip	Additional parameters in model space

obtained from such a sensitivity analysis can conveniently be regarded relative measures of uncertainty. Absolute error estimates from logarithmic space are translated into a standard deviation factor in linear space, such that 1.0 is equal to perfect resolution and 1.1 corresponds to a standard deviation of ~10%. We find that when such linearised error estimates become much larger than unity they are best viewed as guidelines, however. The use of error estimates will be illustrated in the following examples.

We finalise the inverse modelling procedure by calculating the DOI for the resulting output models, an operation which relies on a reweighting of the Jacobian matrix. The computations employ a global and absolute sensitivity threshold value, which has been tuned for operating in logarithmic model/data space (Christiansen and Auken, 2012). For a given model, the DOI calculations consider only the parts of the Jacobian related to observed data, implying that the effect of lateral, spatial or vertical model parameter constraints and *a priori* information is not included. With this type of DOI estimate it is possible to judge when the information in a model is driven by data or heavily dependent on the starting model or specifics of the regularisation.

Limitations due to dimensionality of the forward response and inversion

The functionalities described so far illustrate the general capabilities of the algorithm at its current stage of development, but obviously its inherent limitations should also be considered.

First of all the algorithm base began as a 1D implementation and the whole suite of EM methods are still limited to 1D forward modelling with the exception of 3D sheets. For DC and IP the forward algorithms are present in both 1D and 2D versions and a 3D implementation is close to being complete. Solving the physical problem in 1D can be a limitation for applications such as mineral exploration, whereas studies of sedimentary settings fits well within a 1D modelling envelope (e.g. Auken et al., 2008; Vezzoli et al., 2010).

Second, while being implemented as generally as possible, our regularisation and inversion schemes are fundamentally based on a static formulation. This means that it is not possible to experiment with e.g. Tikhonov-style variable regularisation parameters. However, the least-squares (L2-norm) solution can be changed to use the L1-norm or the sharp boundary formalism by Zhdanov et al. (2000) and Vignoli et al. (2013).

Examples

In the following we show four examples demonstrating the capabilities and versatility of the AarhusInv algorithm. In the examples we show inversions of data collected on the ground, in the ground and in the air. We also illustrate the use of spatial, lateral and vertical constraints. The examples are chosen to illustrate widely varying scales of interest, ranging from small scale engineering type of problems to large regional scale surveys. We further illustrate the use of prior information and provide a synthetic example of joint inversion of mixed type data. Finally we provide a synthetic example inverting an airborne dataset with a 3D sheet model.

On and in the ground: DC and time domain induced polarisation

For our first example we present a novel application of joint 1D LCI inversion of surface time domain induced polarisation (TDIP) data and borehole TDIP data. The TDIP method is a natural and efficient extension of standard DC multi electrode

profiling by simply adding the measurement of the time dependence of discharge after an injection current is turned off. Modelling the complete time decay of each data point in the Cole–Cole formulation (Pelton et al., 1978) allows for extracting additional independent model parameters, often making it possible to discriminate earth structures with an otherwise identical signature. Apart from resistivity, each layer of an IP model includes the parameters τ , C and M_0 . Here m_0 is the magnitude of the chargeability when the injection current is turned off at $t=0$, τ is the decay time constant and C is a constant controlling the frequency dependence of the response. The TDIP implementation is described in full detail by Fiandaca et al. (2012) and includes modelling of the full injection current waveform and low pass filters, which can be a cause of serious modelling error when neglected. Compared to the methodology presented by Fiandaca et al. (2012) we add in this example borehole TDIP data for a joint inversion of two data types sharing a common model space, in order to demonstrate the versatility of the algorithm.

The investigated area is a former Danish landfill site active from the 1950s to the 1980s. During this period the landfill was almost completely unregulated and it was further established without any kind of membranes, leachate capture or isolation systems. Previous studies show that oils and chemical waste from the landfill is contaminating the area by water seepage through the landfill, but the extent of the pollution is largely unknown. Additional details of the survey area are provided by Gazoty et al. (2012). Figure 2 shows the dataset consisting of DC/IP data collected using a gradient array protocol and an electrode spacing of 5 m, as well as DC/IP data from a pole–pole EI-log (Sørensen and Larsen, 1999) collected in a borehole around the centre of the profile. For the logging a measurement was made for every half meter down to 24 m. This combined dataset was 1D LCI inverted for models of 21 layers, discretised in fixed boundaries and utilising lateral and vertical smoothness constraints.

On the model sections in Figure 2 the position of the borehole is indicated near the centre. In the right part of the sections further results for two drillings are superimposed for comparison. From these boreholes it is tempting to conclude that the waste and pollution is likely to be localised to the resistive structure in the vicinity of the boreholes. However, when including the chargeability (m_0) section in the interpretation it becomes clear that the extent of the waste body can possibly be much greater. In fact the results of the full investigation of 13 profiles and 15 boreholes show a very strong correlation between buried waste and chargeability, which is undetectable in terms of resistivity alone. Including log data in a joint inversion contributes complementary information due its perpendicular plane of sampling, introducing a completely different frequency domain kernel since the electrodes are placed in the ground. The result of including this complementary and very detailed vertical information is for all model parameters to become well determined at this position as seen in the right part of Figure 2. In turn the entire profile benefits from this added information, since the use of LCI constraints enable lateral migration of information.

In the air: transient electromagnetic

Most of data being inverted by AarhusInv is airborne data from helicopter and fixed wing systems. To illustrate this key application we show result of an SCI inversion of SkyTEM data (Sørensen and Auken, 2004). The SkyTEM system uses dual transmitter moments to provide unbiased time gates from as early as 6 μ s up to 10 ms (Schamper et al., 2014). This allows for accurate forward modelling, including the effects of the

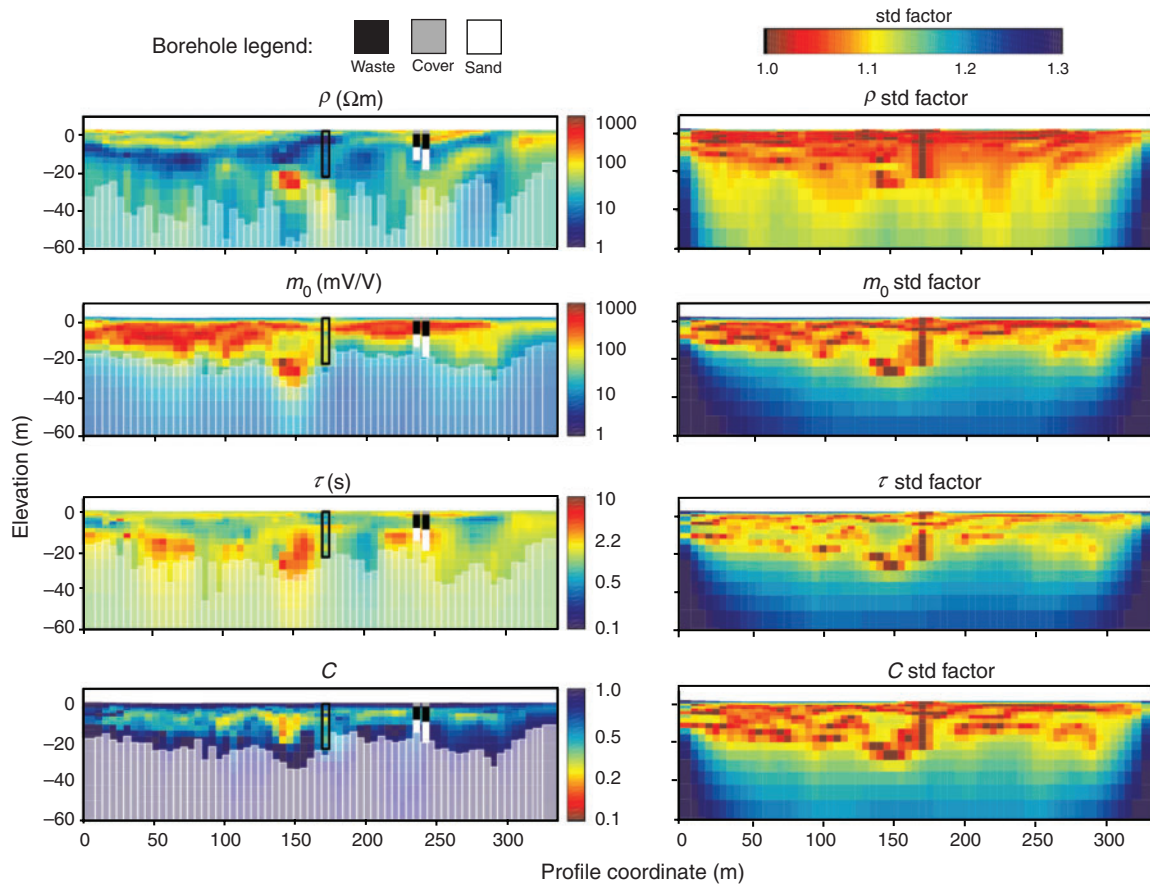


Fig. 2. Joint surface and borehole DC/IP LCI inversion result. The model sections on the left side are faded below the depth on investigation and the right side of the figure shows the corresponding standard deviation sections. The position and depth of the logged borehole included in the inversion is marked by a black square and results from two boreholes are superimposed on the left hand figures.

waveforms of the dual transmitter moments, low pass filters, front gate and finite width gates. For the inversion we use measurements of the vertical component of the secondary field only and include instrument altitude as a model parameter. In the more general case of fixed wing type geometry the algorithm allows for inversion of all field components, including receiver pitch and roll as model parameters (Auken et al., 2009b). We have also implemented inversion for receiver coil response model parameter, allowing for the use of data from time gates as early as $6 \mu\text{s}$ (Schamper et al., 2014).

Our example dataset of 3250 line km was collected in 2009 covering an area of $\sim 820 \text{ km}^2$ intersected by the Danish/German border, having virtually no topography and covering the coast to the North Sea. The survey was conducted to provide a better overall understanding of the hydrogeological setting in the area and to map the fresh/salt water interface in the coastal region. Following data acquisition, all couplings due to man-made installations were removed from the raw dataset and further processed using the methodology of Auken et al. (2009c). The result is a dataset of stacked soundings for each transmitter moment approximately every 25 m. This dataset was jointly inverted for both moments using 19 layer 1D models with fixed layer boundaries and constrained using the SCI methodology. We show the results of the inversion in Figure 3: Figure 3a shows the flight lines of the dataset; Figure 3b, the depth of investigation; Figure 3c, the modelled resistivity at a depth of 74–88 m; and Figure 3d, the model parameter analysis of Figure 3c. From resistivity maps (Figure 3c) it is as possible to identify important features of both regional- and more local scale if zooming into the details. This is

illustrated by marking the extent of two buried valley structures and a large area of salt water intrusion. The geological interpretation of the dataset including cross-sections and average resistivity maps is discussed in detail by Jørgensen et al. (2012).

Mixed data types: magnetic resonance sounding and airborne TEM

For this example we show a feasibility study involving forward modelling, inversion and sensitivity analysis of MRS data in combination with airborne TEM data. The example is intended to illustrate the capabilities of the algorithm on mixed type datasets, utilising multiple modules of the algorithm simultaneously.

The synthetic model of our study is outlined in Table 3 and represents a 20-m thick aquifer situated at a depth of 50 m, covered by dry sands, a till layer and defined at depth by a thick layer of clay. For this synthetic model we consider two types of synthetic data: an airborne TEM sounding and a ground-based MRS sounding. The TEM sounding simulates a SkyTEM system with a 300 m^2 transmitter loop situated at an altitude of 30 m, acquiring data for time gates ranging from $10 \mu\text{s}$ to 1 ms. For the inversion the simulated data is assigned a uniform noise level of 3%, but no actual perturbation is performed. In case of the MRS part of the dataset we consider a simulation with a $100 \text{ m} \times 100 \text{ m}$ square loop. We further set the magnetic field of the earth to 49300 nT at an inclination of 70° and a declination of $+2^\circ$ and utilise pulse moment values ranging from 0.11 to 15.0 As. The synthetically generated sounding was assigned and

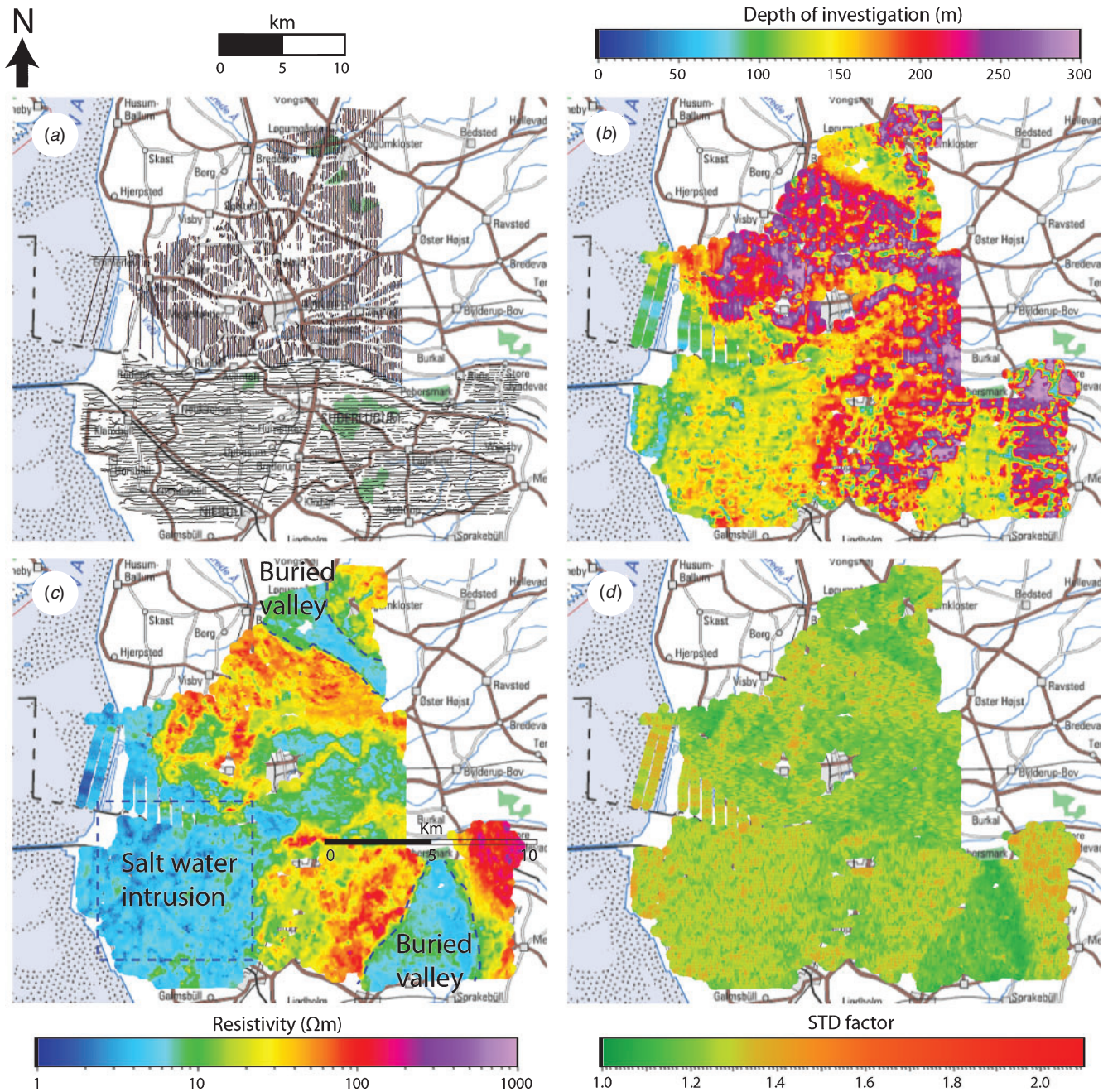


Fig. 3. SkyTEM SCI inversion results. (a) Flight lines of the dataset, (b) depth of investigation, (c) modelled resistivity at a depth of 74–88 m and (d) model parameter analysis of (c).

Table 3. The synthetic model used for mixed modelling of MRS and airborne TEM data.

Layer	Lithology	Resistivity (Ωm)	Thickness (m)	Water content (m ³ /m ³)	T2* (s)	C
1	Till, some water	40	30	0.1	0.1	1
2	Dry sand	300	20	0.02	0.2	1
3	Saturated sand	80	20	0.4	0.2	1
4	Clay	5		0.4	0.02	1

perturbed for a base noise level of 20 nV, with an additional uniform noise contribution of 3%.

Traditionally MRS data has been inverted in what can be referred to as step-wise inversion schemes (e.g. Günther et al.,

2011; Mueller-Petke and Yaramanci, 2010; Behroozmand et al., 2012b). This type of inversion starts by inverting a TEM or DC sounding for a resistivity model, which is then assumed to be the true model in a subsequent inversion for MRS model parameters (water content ratio W and relaxation time $T2^*$). In other words the MRS kernel function, which is a function of the resistivity model, is assumed fixed. Behroozmand et al. (2012a) proposes a joint inversion methodology where the resistivity model parameters are free in the inversion, implying that the MRS kernel has to be updated for each iteration of the inversion requiring a fast numerical implementation of the MRS kernel. In the following we compare the resolution capabilities of these two methods.

In Figure 4, the model results of a traditional step-wise inversion of the simulated data is shown. The figure features dashed blue lines for indicating 68% confidence intervals, as

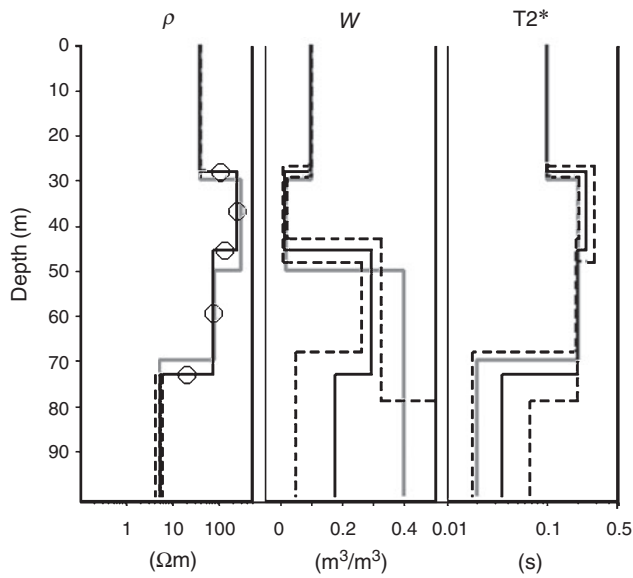


Fig. 4. Results of MRS and airborne TEM step-wise inversion. The grey lines show the true model and the black lines show the inverted model results. The dashed black lines indicate 68% confidence intervals, as obtained from model parameter analysis, with a circle superimposed to indicate uncertainty so large that it goes out of the scale of the figure. We note that for the resistivity the sensitivity analysis is based on TEM data alone.

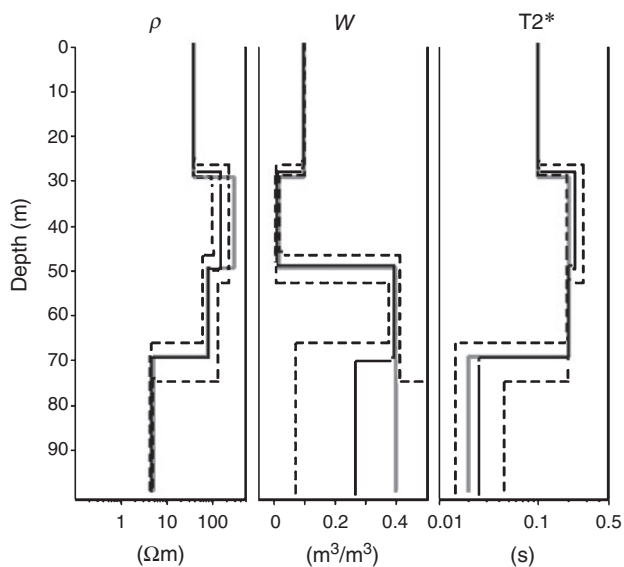


Fig. 5. MRS and airborne TEM full joint inversion results. The grey lines show the true model parameters and the black lines the inverted parameters. The dashed lines indicate 68% confidence intervals, as obtained from model parameter analysis.

obtained from a sensitivity analysis. It is clear that the upper- and lower-most boundaries of the resistivity model are very well resolved, whereas the layering in between these boundaries is completely undetermined. If a noise perturbation had been applied to the TEM data, the obtained model result would have been very far from the true model for the two highly resistive layers. Turning to the MRS model we see that the water content of the synthetic model is well resolved for the top two layers, but underestimated for the lower lying water bearing sand layer with the true value out of range of the model's 68% confidence intervals. This mismatch is caused by the slightly

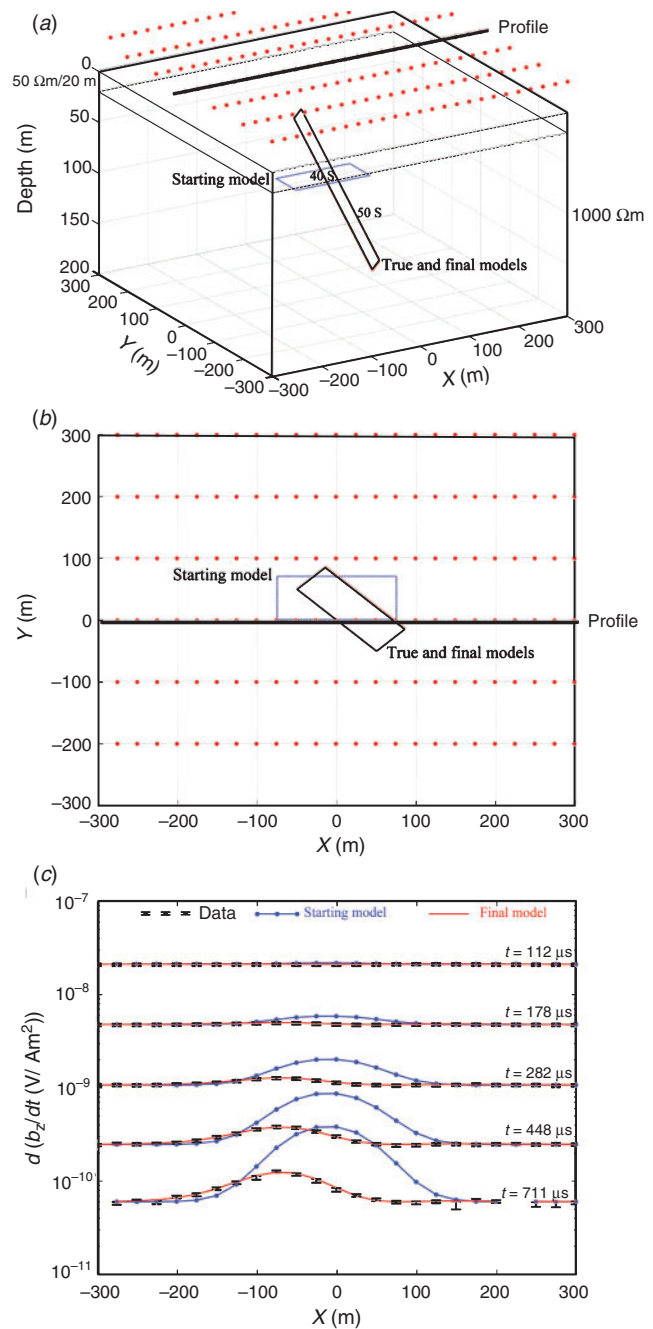


Fig. 6. Thin sheet inversion results where the sheet is buried under a conductive overburden. (a) 3D view of the thin sheets with the starting, true and final estimated models (the last two are confounded), the dots show the airborne TEM sounding locations; (b) 2D top view; (c) data profile with the synthetic generated data (noise has been added at late times), the response of the starting model, and the response of the final model.

wrong layer thicknesses fixed in the resistivity model, which in turn forces the modelled water content to compensate for the MRS kernel function being slightly off. For the bottom layer the inverted water content is found to be even further from the true model, but in this case the deviation can to a larger degree be attributed to a high degree of uncertainty as it is closer to the depth of investigation. In general, T2* values are found to be reasonably well resolved for all layers.

In Figure 5, the result of the joint inversion scheme is shown. The first thing to note is how all layers of the resistivity model have become well resolved, also in the case of the two resistive layers.

Determination of layer thicknesses has improved in particular, due to the combined, complementary information provided by the SkyTEM and MRS signals. In the case of MRS model parameters this point can be seen from the water content model being very accurately reproduced for the top three layers, while the improvement for the deepest lying layer is less pronounced as it is closer to the depth of investigation. For the T2* model the impact of the coupled scheme is very little.

Airborne TEM and sheets inversion

In the AarhusInv code, the forward modelling of thin sheets is based on the algorithm developed by Zhou (1989) with the mathematical formulation from Weidelt (1983). This algorithm calculates the response from several arbitrarily located thin sheets in a conductive layered host. The sheets have both inductive and channelling current modes. If several sheets are used they will be inductively coupled. To speed up the computation the algorithm uses OpenMP to take advantage of multi-processor computer architecture, and an efficient solver has been added to compute the scattered fields for inversion of airborne datasets where many source-receiver locations need to be computed. Furthermore, the algorithm has been extended to include both dipole and finite loop sources, and it calculates responses both in the time and frequency domain as stated in Tables 1 and 2.

We will illustrate the use of this part of AarhusInv on synthetic transient AEM data as shown in Figure 6. The model has a 20 m conductive overburden of 50 Ωm , covering a resistive halfspace of 1000 Ωm . The sheet is in the resistive host and has a conductance of 50 S, a top depth of 30 m, a maximum depth of 175 m, and both its dip and strike angles are 45° (Figure 6a). The simulated AEM dataset has a line spacing of 100 m with a sounding spacing of 20 m along the lines (Figure 6b) and z-component data only. The flight altitude is 30 m and recorded times span from $\sim 10\ \mu\text{s}$ to a few ms depending on the noise. Random noise at a slope of $t^{-1/2}$ and a noise level of 1 nV/m² at 1 ms was added to the data (Schamper et al., 2014). Figure 6c illustrates the fit obtained after inversion with some of the recorded times along the central profile. The starting model parameters are indicated in the figure. The parameters in the inversion are sheet conductance, dip, strike, layered model parameters and flight altitude. In the present case, the sheet is well determined with the TEM method and the final estimated model is well recovered and almost identical to the true model as is also indicated by the parameter determination (not shown here).

Conclusions

We have presented an overview of a proven, versatile and flexible production inversion algorithm, capable of inverting most electric and electromagnetic data types and supporting most instruments normally used within the field of near surface geophysics. The algorithm is freely available for academic use and provides the user with freedom to specify arbitrary 3D regularisation constraints, include any amount of prior information and invert for mixed type datasets. Our implementation focuses on consistently accurate system forward modelling independent of data type and instrument, which not only ensures accuracy, but can also be regarded a prerequisite for joint inversion of data collected using instruments of different transfer function. The implementation is modular, meaning that the bulk of the algorithm is independent of data type, making it very easy to add support for new types of data. Calculation of both model parameter sensitivity analysis and depth of investigation is a key feature and it is handled automatically regardless of configuration and data types.

The versatility of the algorithm is illustrated by four different examples. First, we showed the joint inversion of a resistivity/time-domain IP dataset with electrodes both located in the ground and on the surface. This example provides an illustration of how including Cole–Cole parameters in the model greatly improves the delineation of a former landfill. Second, we have shown results of a large scale airborne TEM survey where the combined information from maps of average resistivity, depth-of-investigation and model parameter analysis improves the understanding of the underlying geology. Third, we have shown a synthetic example where we jointly invert Airborne TEM data with ground-based MRS data. These two model-spaces are only vaguely related, but we show how the mutual information significantly improves the resolution of both the resistivity- and the water content model. In the fourth example we showed a synthetic example inverting Airborne TEM data with a 3D sheets model.

Acknowledgements

Over the years the development of the code has been supported by several different research projects. The most prominent has been the HOBE Center of Excellence (Villum Kahn Rasmussen Foundation) and the four projects RiskPoint, NICA, CO2GS and HyGEM, all larger research projects funded by the Danish Counsel for Strategic Research. Also the Nature Agency under the Danish Ministry of the Environment has greatly supported our work as an integrated part of the national groundwater mapping program. Lastly, we have to thank numerous students who had to suffer long nights with new implementations not always working as expected in the first beta releases.

References

- Auken, E., and Christiansen, A. V., 2004, Layered and laterally constrained 2D inversion of resistivity data: *Geophysics*, **69**, 752–761. doi:10.1190/1.1759461
- Auken, E., Nebel, L., Sørensen, K. I., Breiner, M., Pellerin, L., and Christensen, N. B., 2002, EMMA – a geophysical training and education tool for electromagnetic modeling and analysis: *Journal of Environmental & Engineering Geophysics*, **7**, 57–68. doi:10.4133/JEEG7.2.57
- Auken, E., Christiansen, A. V., Jacobsen, B. H., Foged, N., and Sørensen, K. I., 2005, Piecewise 1D laterally constrained inversion of resistivity data: *Geophysical Prospecting*, **53**, 497–506. doi:10.1111/j.1365-2478.2005.00486.x
- Auken, E., Christiansen, A. V., Jacobsen, L., and Sørensen, K. I., 2008, A resolution study of buried valleys using laterally constrained inversion of TEM data: *Journal of Applied Geophysics*, **65**, 10–20. doi:10.1016/j.jappgeo.2008.03.003
- Auken, E., Christiansen, A. V., Viezzoli, A., Fitzpatrick, A., Cahill, K., Munday, T., and Berens, V., 2009a, Investigation on the groundwater resources of the South Eyre Peninsula, South Australia, determined from laterally constrained inversion of TEMPEST data: ASEG Extended Abstracts 2009, 1–5.
- Auken, E., Christiansen, A. V., Viezzoli, A., Fitzpatrick, A., and Munday, T., 2009b, Laterally constrained inversion of TEMPEST data from Eyre Peninsula area, South Australia: 15th European Meeting of Environmental and Engineering Geophysics, 2009.
- Auken, E., Christiansen, A. V., Westergaard, J. A., Kirkegaard, C., Foged, N., and Viezzoli, A., 2009c, An integrated processing scheme for high-resolution airborne electromagnetic surveys, the SkyTEM system: *Exploration Geophysics*, **40**, 184–192. doi:10.1071/EG08128
- Balch, S. J., Boyko, W. P., and Paterson, N. R., 2003, The AeroTEM airborne electromagnetic system: *The Leading Edge*, **22**, 562–566. doi:10.1190/1.1587679
- Behroozmand, A. A., Auken, E., Fiandaca, G., and Christiansen, A. V., 2012a, Improvement in MRS parameter estimation by joint and laterally constrained inversion of MRS and TEM data: *Geophysics*, **74**, WB191–WB200.
- Behroozmand, A. A., Auken, E., Fiandaca, G., Christiansen, A. V., and Christensen, N. B., 2012b, Efficient full decay inversion of MRS data with

- a stretched-exponential approximation of the T2* distribution: *Geophysical Journal International*, **190**, 900–912. doi:10.1111/j.1365-246X.2012.05558.x
- Bracewell, R. N., 1986, *The Fourier transform and its applications* (2nd edition): McGraw-Hill, Inc.
- Brodie, R., and Sambridge, M., 2006a, A holistic approach to inversion of frequency-domain airborne EM data: *Geophysics*, **71**, G301–G312. doi:10.1190/1.2356112
- Brodie, R., and Sambridge, M., 2006b, A holistic approach to inversion of time-domain airborne EM: ASEG Extended Abstracts 2006, 1–4.
- Christensen, N. B., 1990, Optimized fast Hankel transform filters: *Geophysical Prospecting*, **38**, 545–568. doi:10.1111/j.1365-2478.1990.tb01861.x
- Christensen, N. B., 2002, A generic 1-D imaging method for transient electromagnetic data: *Geophysics*, **67**, 438–447. doi:10.1190/1.1468603
- Christensen, N. B., and Auken, E., 1992, Simultaneous electromagnetic layered model analysis: *Proceedings of the Interdisciplinary Inversion Workshop 1*, Geoskifter, 49–56.
- Christiansen, A. V., and Auken, E., 2012, A global measure for depth of investigation: *Geophysics*, **77**, WB171–WB177.
- Christiansen, A. V., Auken, E., and Viezzoli, A., 2011, Quantification of modeling errors in airborne TEM caused by inaccurate system description: *Geophysics*, **76**, F43–F52. doi:10.1190/1.3511354
- Cox, L. H., Wilson, G. A., and Zhdanov, M. S., 2010, 3D inversion of airborne electromagnetic data using a moving footprint: *Exploration Geophysics*, **41**, 250–259. doi:10.1071/EG10003
- d'Ozouville, N., Auken, E., Sørensen, K. I., Violette, S., Marsily, G. D., Defontaine, B., and Merlen, G., 2008, Extensive perched aquifer and structural implications revealed by 3D resistivity mapping in a Galapagos volcano: *Earth and Planetary Science Letters*, **269**, 518–522. doi:10.1016/j.epsl.2008.03.011
- Danielsen, J. E., Auken, E., Jørgensen, F., Søndergaard, V. H., and Sørensen, K. I., 2003, The application of the transient electromagnetic method in hydrogeophysical surveys: *Journal of Applied Geophysics*, **53**, 181–198. doi:10.1016/j.jappgeo.2003.08.004
- Effersø, F., Auken, E., and Sørensen, K. I., 1999, Inversion of band-limited TEM responses: *Geophysical Prospecting*, **47**, 551–564. doi:10.1046/j.1365-2478.1999.00135.x
- Fiandaca, G., Auken, E., Gazoty, A., and Christiansen, A. V., 2012, Time-domain induced polarization: full-decay forward modeling and 1D laterally constrained inversion of Cole-Cole parameters: *Geophysics*, **77**, E213–E225. doi:10.1190/geo2011-0217.1
- Fiandaca, G., Ramm, J., Binley, A., Gazoty, A., Christiansen, A. V., and Auken, E., 2013, Resolving spectral information from time domain induced polarization data through 2-D inversion: *Geophysical Journal International*, **192**, 631–646. doi:10.1093/gji/ggs060
- Fitterman, D. V., and Anderson, W. L., 1987, Effect of transmitter turn-off time on transient soundings: *Geophysical Prospecting*, **24**, 131–146. doi:10.1016/0016-7142(87)90087-1
- Gazoty, A., Fiandaca, G., Pedersen, J., Auken, E., and Christiansen, A. V., 2012, Mapping of landfills using time-domain spectral induced polarization data: the Eskelund case study: *Near Surface Geophysics*, **10**, 563–574.
- Gribenko, A., Wan, L., and Zhdanov, M. S., 2010, Three-dimensional inversion of magnetotelluric data for complex resistivity: *Proceedings of the CEMI Annual Meeting*, 269–294.
- Günther, T., Rücker, C., and Spitzer, K., 2006, Three-dimensional modelling and inversion of dc resistivity data incorporating topography – II. Inversion: *Geophysical Journal International*, **166**, 506–517. doi:10.1111/j.1365-246X.2006.03011.x
- Günther, T., Liebau, J., Akca, I., and Mueller-Petke, M., 2011, Block joint inversion (BJI) of MRS and DC resistivity soundings for aquifer imaging at the North Sea island, Borkum: Near Surface 2011 – The 17th European Meeting of Environmental and Engineering Geophysics, 2011.
- Hertrich, M., Braun, M., and Yaramanci, U., 2005, Magnetic resonance soundings with separated transmitter and receiver loops: *Near Surface Geophysics*, **3**, 141–154.
- Johansen, H. K., and Sørensen, K. I., 1979, Fast Hankel transforms: *Geophysical Prospecting*, **27**, 876–901. doi:10.1111/j.1365-2478.1979.tb01005.x
- Jørgensen, F., and Sanderson, P. B. E., 2006, Buried and open tunnel valleys in Denmark – erosion beneath multiple ice sheets: *Quaternary Science Reviews*, **25**, 1339–1363. doi:10.1016/j.quascirev.2005.11.006
- Jørgensen, F., Scheer, W., Thomsen, S., Sonnenborg, T. O., Hinsby, K., Wiederhold, H., Schamper, C., Roth, B., Kirsch, R., and Auken, E., 2012, Transboundary geophysical mapping of geological elements and salinity distribution critical for the assessment of future sea water intrusion in response to sea level rise: *Hydrology and Earth System Sciences*, **16**, 1845–1862. doi:10.5194/hess-16-1845-2012
- Kemna, A., Binley, A., Ramirez, A., and Daily, W., 2000, Complex resistivity tomography for environmental applications: *Chemical Engineering Journal*, **77**, 11–18. doi:10.1016/S1385-8947(99)00135-7
- Kirkegaard, C., and Auken, E., 2014, A parallel, scalable and memory efficient inversion code for very large scale airborne EM surveys: *Geophysical Prospecting*, in press.
- Knight, J. H., and Raiche, A. P., 1982, Transient electromagnetic calculations using the Gaver-Stehfest inverse Laplace transform method: *Geophysics*, **47**, 47–50. doi:10.1190/1.1441280
- Lane, R., Green, A. G., Golding, C., Owers, M., Pik, P., Plunkett, C., Sattel, D., and Thorn, B., 2000, An example of 3D conductivity mapping using the TEMPEST airborne electromagnetic system: *Exploration Geophysics*, **31**, 162–172. doi:10.1071/EG00162
- Loke, M. H., 2011, RES3DINV: Geotomo software. Available at www.geoelectrical.com
- Loke, M. H., and Barker, R. D., 1996, Rapid least squares inversion of apparent resistivity pseudosections by a quasi-Newton method: *Geophysical Prospecting*, **44**, 131–152. doi:10.1111/j.1365-2478.1996.tb00142.x
- Loke, M. H., Chambers, J. E., and Ogilvy, R. D., 2006, Inversion of 2D spectral induced polarization imaging data: *Geophysical Prospecting*, **54**, 287–301. doi:10.1111/j.1365-2478.2006.00537.x
- Macnae, J. C., Smith, R., Polzer, B. D., Lamontagne, Y., and Klinkert, P. S., 1991, Conductivity-depth imaging of airborne electromagnetic step-response data: *Geophysics*, **56**, 102–114. doi:10.1190/1.1442945
- Marquardt, D., 1963, An algorithm for least squares estimation of nonlinear parameters: *SIAM Journal of the Society for Industrial and Applied Mathematics*, **11**, 431–441. doi:10.1137/0111030
- Menke, W., 1989, *Geophysical data analysis discrete inverse theory*: Academic Press.
- Mohnke, O., and Yaramanci, U., 2002, Smooth and block inversion of surface NMR amplitudes and decay times using simulated annealing: *Journal of Applied Geophysics*, **50**, 163–177. doi:10.1016/S0926-9851(02)00137-4
- Møller, I., Verner, H., Søndergaard, V. H., Flemming, J., Auken, E., and Christiansen, A. V., 2009, Integrated management and utilization of hydrogeophysical data on a national scale: *Near Surface Geophysics*, **7**, 647–659.
- Mueller-Petke, M., and Yaramanci, U., 2010, QT inversion – comprehensive use of the complete surface NMR data set: *Geophysics*, **75**, WA199–WA209. doi:10.1190/1.3471523
- Newman, G. A., and Alumbaugh, D. L., 1997, Three-dimensional massively parallel electromagnetic inversion – I. Theory: *Geophysical Journal International*, **128**, 345–354. doi:10.1111/j.1365-246X.1997.tb01559.x
- Newman, G. A., Hohmann, G. W., and Anderson, W. L., 1986, Transient electromagnetic response of a three-dimensional body in a layered earth: *Geophysics*, **51**, 1608–1627. doi:10.1190/1.1442212
- Oldenburg, D. W., and Jones, F. H. M., 2011a, DCIP3D (Inversion for Applied Geophysics): University of British Columbia Geophysical Inversion Facility. Available at www.eos.ubc.ca/ubcgif/iag/
- Oldenburg, D. W., and Jones, F. H. M., 2011b, EMIDFM (Inversion for Applied Geophysics): University of British Columbia Geophysical Inversion Facility. Available at www.eos.ubc.ca/ubcgif/iag/
- Oldenburg, D. W., and Jones, F. H. M., 2011c, EM1DTM (Inversion for Applied Geophysics): University of British Columbia Geophysical Inversion Facility. Available at www.eos.ubc.ca/ubcgif/iag/
- Oldenburg, D. W., and Li, Y., 1994, Inversion of induced polarization data: *Geophysics*, **59**, 1327–1341. doi:10.1190/1.1443692
- Oldenburg, D. W., Haber, E., and Shekhtman, R., 2013, Three dimensional inversion of multisource time domain electromagnetic data: *Geophysics*, **78**, E47–E57. doi:10.1190/geo2012-0131.1

- Pelton, W. H., Ward, S. H., Hallof, P. G., Sill, W. R., and Nelson, P. H., 1978, Mineral discrimination and removal of inductive coupling with multifrequency induced-polarization: *Geophysics*, **43**, 588–609. doi:10.1190/1.1440839
- Podgorski, J. E., Auken, E., Schamper, C., Christiansen, A. V., Kalscheuer, T., and Green, A. G., 2013, Processing and inversion of commercial helicopter time-domain electromagnetic data for environmental assessments and geologic and hydrologic mapping: *Geophysics*, **78**, E149–E159. doi:10.1190/geo2012-0452.1
- Reid, J. E., Munday, T., and Fitzpatrick, A., 2007, High-resolution airborne electromagnetic surveying for dryland salinity management: the Toolibin Lake SkyTEM case study, W.A.: ASEG Extended Abstracts 2007, 1–5.
- Rücker, C., Günther, T., and Spitzer, K., 2006, Three-dimensional modelling and inversion of dc resistivity data incorporating topography – I. Modelling: *Geophysical Journal International*, **166**, 495–505. doi:10.1111/j.1365-246X.2006.03010.x
- Santos, F. A. M., 2004, 1-D laterally constrained inversion of EM34 profiling data: *Journal of Applied Geophysics*, **56**, 123–134. doi:10.1016/j.jappgeo.2004.04.005
- Sato, H. K., 2000, Potential field from a dc current source arbitrarily located in a nonuniform layered medium: *Geophysics*, **65**, 1726–1732. doi:10.1190/1.1444857
- Schamper, C., Auken, E., and Kirkegaard, C., 2013, 3D sheets inversion with accurate modeling of AEM systems: SAGA AEM, South Africa, 1–2.
- Schamper, C., Auken, E., and Sørensen, K. I., 2014, Coil response inversion for very early time modelling of helicopter-borne time-domain electromagnetic data and mapping of near-surface geological layers: *Geophysical Prospecting*, **62**, 658–674. doi:10.1111/1365-2478.12104
- Sengpiel, K. P., and Siemon, B., 2000, Advanced inversion methods for airborne electromagnetic exploration: *Geophysics*, **65**, 1983–1992. doi:10.1190/1.1444882
- Siemon, B., Stuntebeck, C., Sengpiel, K. P., Röttger, B., Rehli, H., and Eberle, D. G., 2002, Investigation of hazardous waste sites and their environment using BGR helicopter-borne geophysical system: *Journal of Environmental & Engineering Geophysics*, **7**, 169–181. doi:10.4133/JEEG7.4.169
- Sørensen, K. I., and Auken, E., 2004, SkyTEM – a new high-resolution helicopter transient electromagnetic system: *Exploration Geophysics*, **35**, 191–199.
- Sørensen, K. I., and Larsen, F., 1999, Ellog auger drilling: 3-in-one method for hydrogeological data collection: *Ground Water Monitoring and Remediation*, **19**, 97–101. doi:10.1111/j.1745-6592.1999.tb00245.x
- Sørensen, K. I., Auken, E., Christensen, N. B., and Pellerin, L., 2005, An integrated approach for hydrogeophysical investigations: new technologies and a case history, in D. K. Butler, ed., *Near-surface geophysics*, Part II: SEG, 585–603.
- Tarantola, A., and Valette, B., 1982a, Generalized nonlinear inverse problems solved using a least squares criterion: *Reviews of Geophysics and Space Physics*, **20**, 219–232. doi:10.1029/RG020i002p00219
- Tarantola, A., and Valette, B., 1982b, Inverse problems = quest for information: *Journal of Geophysics*, **50**, 159–170.
- Tartaras, E., Zhdanov, M. S., Wada, K., Saito, A., and Hara, T., 2000, Fast imaging of TDEM data based on S-inversion: *Journal of Applied Geophysics*, **43**, 15–32. doi:10.1016/S0926-9851(99)00030-0
- Thomsen, R., Søndergaard, V. H., and Sørensen, K. I., 2004, Hydrogeological mapping as a basis for establishing site-specific groundwater protection zones in Denmark: *Hydrogeology Journal*, **12**, 550–562. doi:10.1007/s10040-004-0345-1
- Viezzoli, A., Christiansen, A. V., Auken, E., and Sørensen, K. I., 2008, Quasi-3D modeling of airborne TEM data by spatially constrained inversion: *Geophysics*, **73**, F105–F113. doi:10.1190/1.2895521
- Viezzoli, A., Munday, T., Auken, E., and Christiansen, A. V., 2010, Accurate quasi 3D versus practical full 3D inversion of AEM data – the Bookpurnong case study: *Preview*, **149**, 23–31.
- Vignoli, G., Fiandaca, G., Christiansen, A. V., Kirkegaard, C., and Auken, E., 2013, Sharp Spatially Constrained Inversion (sSCI) with applications to transient electromagnetic data: *Geophysical Prospecting*, in press.
- Wannamaker, P. E., Hohmann, G. W., and SanFilippo, W. A., 1984, Electromagnetic modeling of three-dimensional bodies in layered earths using integral equations: *Geophysics*, **49**, 60–74. doi:10.1190/1.1441562
- Ward, S. H., and Hohmann, G. W., 1988, Electromagnetic theory for geophysical applications, in M. N. Nabighian, ed., *Electromagnetic methods in applied geophysics*, Vol. 1: Society of Exploration Geophysicists, 131–311.
- Weichman, P. B., Lavelly, E. M., and Ritzwoller, M. H., 2000, Theory of surface nuclear magnetic resonance with applications to geophysical imaging problems: *Physical Review E: Statistical Physics, Plasmas, Fluids, and Related Interdisciplinary Topics*, **62**, 1290–1312. doi:10.1103/PhysRevE.62.1290
- Weidelt, P., 1983, The harmonic and transient electromagnetic response of a thin dipping dike: *Geophysics*, **48**, 934–952. doi:10.1190/1.1441520
- Wisén, R., and Christiansen, A. V., 2005, Laterally and mutually constrained inversion of surface wave seismic data and resistivity data: *Journal of Environmental & Engineering Geophysics*, **10**, 251–262. doi:10.2113/JEEG10.3.251
- Witherly, K. E., Irvine, R. J., and Morrison, E., 2004, The Geotech VTEM time domain helicopter EM system: ASEG Extended Abstracts 2004, 1–4.
- Xiong, Z., 1989, Electromagnetic fields of electric dipoles embedded in a stratified anisotropic earth: *Geophysics*, **54**, 1643–1646. doi:10.1190/1.1442633
- Yoshioka, K., and Zhdanov, M. S., 2005, Three-dimensional nonlinear regularized inversion of the induced polarization data based on the Cole-Cole model: *Physics of the Earth and Planetary Interiors*, **150**, 29–43. doi:10.1016/j.pepi.2004.08.034
- Zhdanov, M. S., and Keller, G. V., 1994, *The geoelectrical methods in geophysical exploration*: Elsevier.
- Zhdanov, M. S., Fang, S., and Hursán, G., 2000, Electromagnetic inversion using quasi-linear approximation: *Geophysics*, **65**, 1501–1513. doi:10.1190/1.1444839
- Zhou, Q., 1989, Audio-frequency electromagnetic tomography for reservoir evaluation: Ph.D. dissertation, Lawrence Berkeley Laboratory, University of California.

Appendix A

1D EM forward calculation

The type of problem we consider consist of a given instrument source, receiver and layered half-space for which to solve Maxwell's equations. We do this in order to calculate some or all of the electromagnetic field components, or their time derivatives, at the position of the receiver. This type of calculation is normally performed in the frequency domain and can be formulated to exploit symmetry by choosing the gauge leading to the Schelkunoff potential formulation. In the following analysis, we closely follow Ward and Hohmann (1988). In the Schelkunoff formalism we operate on the electric and magnetic vector potentials \mathbf{A} and \mathbf{F} from which the actual electromagnetic fields can be determined by means of differentiation. This formulation is desirable since the vector potentials point in the direction of a source with a convenient geometry, allowing for calculation of all EM field components from just a single non-zero component of either \mathbf{A} or \mathbf{F} . In cases of more complicated geometry the problem can be reduced to solving multiple simple problems by means of mode decomposition.

In equation A-1, we show the characteristic type of equation to be solved in order to calculate the non-zero component of the vector potentials, here in the case of a z -directed magnetic source.

$$F(x, y, z) \propto \hat{z} \iint_{-\infty}^{\infty} f(x, y, z, k_x^2 + k_y^2) e^{-i(k_x x + k_y y)} dk_x dk_y \quad (\text{A-1})$$

where $\hat{z} = i\mu\omega$, μ is the magnetic permeability, ω is the angular frequency, k_x and k_y are the wavenumbers in the x - and y -directions.

We recognise this double integral as an inverse 2D Fourier transform, which can be reduced to a single integral by applying an inverse Hankel transform instead. This is possible since f is cylinder symmetric given its dependence on $k_x^2 + k_y^2$ and allows for the equation to be rewritten in simpler form:

$$F(\rho, z) \propto \hat{z} \int_0^{\infty} f(\lambda, z) \cdot \lambda \cdot J_0(\lambda\rho) d\lambda \quad (\text{A-2})$$

where λ is the space frequency, and J_0 is the 0th order Bessel function. This type of inverse Hankel transform integral can be evaluated very efficiently using digital filter methods as described by Johansen and Sørensen (1979) and Christensen (1990). Given the ability to efficiently solve inverse Hankel transform type integrals allows for fast calculation of any EM field component, by simple means of differentiation of the vector potential equations. In the calculation of the type of integral in equation A-2 the most time consuming part becomes the evaluation of the integrand function f . This function includes a frequency dependent reflection coefficient, essentially accounting for the amplitudes of up- and down-going damped waves within the layered half-space. This is calculated from a recurrence relation going up through the layering which becomes the effective bottlenecking term, making the calculation time scale linearly with the number of layers in the half space. In the case of frequency domain data these are simply the transmitted frequencies of the system, whereas the frequency space needs to be more systematically sampled for time domain problems. In this latter case we solve for a data type specific number of logarithmically spaced frequencies per decade and transform into the time domain using an inverse sine/cosine digital filter transform (Johansen and Sørensen, 1979; Newman et al., 1986). This approach is much more efficient than a standard inverse fast Fourier transform and for late times we also find it more stable and accurate than the faster Gaver-Stehfest inverse Laplace transform (Knight and Raiche, 1982). To get to the final time domain result from the discretely transformed frequency domain data we apply an interpolating bicubic spline to obtain results for the particular points in time of interest.

For the accuracy of the resulting responses we note that this is determined mainly by the sampling density of the digital filters. Higher density implies more computations, meaning that a performance/accuracy compromise has to be made. We allow for the user to manually tune this trade off, but provide default settings for an error of around 0.3% for frequencies up to 100–200 kHz and for a time domain error of less than 1% for times as early as 4 μ s. These frequencies and times are somehow dependent on the overall conductivity of the ground and thus high frequencies and early times are more inaccurate for very high resistivities than for low resistivities.

Ever since the codebase was started more than 15 years ago, all responses and common routines have been routinely validated against both analytical expressions and other forward modelling algorithms.

Modelling the system transfer function for TEM systems

An important aspect of modelling a complete TEM system is accounting for the transmitter waveform. In the case of a step function this is done directly by integration in the frequency domain (Bracewell, 1986), while the general case of arbitrary waveform is handled by convolution in the time domain using the approach of Fitterman and Anderson (1987). These authors show that an arbitrary waveform can be accounted for by a simple rewrite of the convolution so it is expressed as a sum over a numerical differentiation of a piece-wise linear waveform.

Of equal importance is accounting for the receiver frequency characteristics. Not only does a receiver coil itself have a frequency characteristic, but further low-pass filters are typically also applied and both can have a significant influence on the measured signal over the dynamic range of interest. Effersø et al. (1999) describes how low and high pass filtering are implemented in the frequency domain before transforming to the time domain. This is done by a simple multiplication of a filter response function, here in the form of a Butterworth filter, with the same approach used for modelling of low pass filters for TDIP responses. The effect of finite gate width is included in the modelling by integrating cubic spline functions over the width of the gate. If finite gates are not used the response at the gate centre times are calculated from a local interpolation using cubic splines. Some instruments further utilise a special gate right after the receiver coil. This gate serves to prevent strong primary fields from saturating the receiver amplifiers during transmitter turn on and it is modelled by convolving a shifted heavy side function with the step response.

Using SkyTEM as an example the full procedure for forward modelling the response becomes: (1) the filter effect of the receiver coil is modelled in the frequency domain as a simple product; (2) the frequency domain response is transformed to the time domain using a Hankel transform; (3) the front gate is convolved with the step response; (4) low pass filters in the receiver instrument are applied as a new convolution; (5) a piece-wise linear waveform is applied by numerical differentiation; and finally (6) gates are calculated by integrating the response over the length of the gates.

Appendix B

Least-squares inversion

The inversion is performed iteratively, by following the established practice of linearised approximation of the non-linear forward mapping of the model to the data space, by the first term of the Taylor expansion (Menke, 1989; Auken et al., 2005). The $n+1$ th update of the model vector \mathbf{m}_{n+1} is obtained by:

$$\mathbf{m}_{n+1} = \mathbf{m}_n + [\mathbf{G}_n^{\prime T} \mathbf{C}'^{-1} \mathbf{G}_n' + \lambda_n \mathbf{I}]^{-1} \cdot [\mathbf{G}_n^{\prime T} \mathbf{C}'^{-1} \delta \mathbf{d}'_n] \quad (\text{B-1})$$

where the Jacobian \mathbf{G}_n' , the data vector update $\delta \mathbf{d}'_n$ and the covariance matrix \mathbf{C}' incorporate both the *a priori* and the roughness constraints and are defined as:

$$\mathbf{G}_n' = \begin{bmatrix} \mathbf{G}_n \\ \mathbf{P} \\ \mathbf{R} \end{bmatrix} \quad (\text{B-2})$$

$$\delta \mathbf{d}'_n = \begin{bmatrix} \delta \mathbf{d}_n \\ \delta \mathbf{m}_n \\ \delta \mathbf{r}_n \end{bmatrix} = \begin{bmatrix} \mathbf{d}_n - \mathbf{d}_{obs} \\ \mathbf{m}_n - \mathbf{m}_{prior} \\ -\mathbf{R}\mathbf{m}_n \end{bmatrix} \quad (\text{B-3})$$

$$\mathbf{C}' = \begin{bmatrix} \mathbf{C}_{obs} & 0 & 0 \\ 0 & \mathbf{C}_{prior} & 0 \\ 0 & 0 & \mathbf{C}_R \end{bmatrix} \quad (\text{B-4})$$

In equation B-2, \mathbf{G}_n represents the Jacobian of the forward mapping. For 1D LCI/SCI solutions the matrix \mathbf{G}_n is computed by differentiation of forward responses \mathbf{F}_{1D} : $\mathbf{G}_n^{i,j} = (\mathbf{F}_{1D}^i(\mathbf{m} + \Delta \mathbf{m}_j) - \mathbf{F}_{1D}^i(\mathbf{m})) / (\Delta \mathbf{m}_j)$, for datum i and model parameter j . On the contrary, in the 2D DC/IP implementation the Jacobian is computed with the adjoint method approach (Fiandaca et al., 2013). \mathbf{P} is the matrix with dimension $N_m \times N_m$ (N_m being the number of model parameters), necessary to impose the constraints on the *a priori* values. \mathbf{R} is the roughness matrix, in which each row represents one roughness constraint (each row is zero everywhere except for the two elements corresponding to constrained parameters, elements being equal to 1 and -1).

The constraints also appear as extra terms in the definition of the data vector update $\delta \mathbf{d}'_n$ (equation B-3), that is composed of the distance $\delta \mathbf{d}_n$ between the n th forward response \mathbf{d}_n and the observed data \mathbf{d}_{obs} , the distance $\delta \mathbf{m}_n$ between the n th model vector \mathbf{m}_n and the *a priori* model vector \mathbf{m}_{prior} (used also as starting model for the iterative procedure) and the roughness of the n th model vector $\delta \mathbf{r}_n = -\mathbf{R}\mathbf{m}_n$.

The covariance matrix \mathbf{C}' of equation B-4 is defined in terms of the covariance on the observed data \mathbf{C}_{obs} , the covariance on the *a priori* information \mathbf{C}_{prior} and the covariance on the roughness constraints \mathbf{C}_R . All three matrices are considered diagonal; the elements of \mathbf{C}_{prior} and \mathbf{C}_R control the strength of the constraints, while the elements of \mathbf{C}_{obs} reflect the noise content of the data.

The matrices \mathbf{P} , \mathbf{R} , \mathbf{C}_{prior} and \mathbf{C}_R , as well as the vectors $\delta \mathbf{m}_n$ and $\delta \mathbf{r}_n$ are split in two parts in order to account for prior/roughness constraints on both the primary parameters (e.g. resistivity and thickness) and on depths. In fact, the depths are not included directly in the model space, and a special formulation of the matrices is needed to include the depth prior/roughness constraints in equation B-1 (see Auken et al. (2005) for details).

In equation B-1, the parameter λ_n is the Marquardt damping parameter (Marquardt, 1963), iteratively updated to stabilise the inversion process through an adaptive algorithm that damps the step size. This algorithm uses as damping value λ_n the maximum diagonal value of the $\mathbf{G}_n^{\prime T} \mathbf{C}'^{-1} \mathbf{G}_n'$ matrix, reduced by an iterative-dependent scaling factor f_n :

$$\lambda_n = \max \text{diag}(\mathbf{G}_n^{\prime T} \mathbf{C}'^{-1} \mathbf{G}_n') \cdot f_n \quad (\text{B-5})$$

The damping is used to stabilise the solution of the linear system of equation B-1, but a constraint on the 'step size' of the iteration, i.e. the size of the model update $\mathbf{m}_{n+1} - \mathbf{m}_n$, is also imposed through f_n (the step size is reduced by increasing f_n). When increasing the iteration number n , the scaling factor f_n is decreased and the step size is increased ensuring a robust and efficient damping scheme.

The object function minimised by equation B-1 is expressed by

$$\mathbf{Q} = \left(\frac{[\delta \mathbf{d}'^T \mathbf{C}'^{-1} \delta \mathbf{d}']}{N_d + N_m + N_R} \right)^{\frac{1}{2}} \quad (\text{B-6})$$

in which N_d , N_m , N_R represent the number of data points, the number of model parameters and the number of constraints. The output models are then balanced between the data (through the forward response, i.e. the physics), the *a priori* constraints and the roughness constraints.

Finally the covariance of the estimator error \mathbf{C}_{est} (Tarantola and Valette, 1982b) is used in AarhusInv to estimate the resolution of the inverted model by using its expression for linear mappings on the last iteration N_{ite} :

$$\mathbf{C}_{est} = (\mathbf{G}_{N_{ite}}^{\prime T} \mathbf{C}'^{-1} \mathbf{G}_{N_{ite}}')^{-1} \quad (\text{B-7})$$